Highly repeatable nanoscale phase coexistence in vanadium dioxide films

T. J. Huffman, D. J. Lahneman, S. L. Wang, T. Slusar, Bong-Jun Kim, Hyun-Tak Kim, and M. M. Qazilbash

Phys. Rev. B **97**, 085146 — Published 23 February 2018

DOI: 10.1103/PhysRevB.97.085146

Highly repeatable nanoscale phase coexistence in vanadium dioxide films

T. J. Huffman[1], D. J. Lahneman[1], S. L. Wang[1], T. Slusar[2], Bong-Jun Kim[2], Hyun-Tak Kim[2,3] and M. M. Qazilbash[1,*]

[1]Department of Physics, College of William and Mary, Williamsburg, Virginia 23187-8795, USA

[2]Metal-Insulator Transition Lab, Electronics & Telecommunications Research Institute, Daejeon 34129, Republic of Korea

[3]School of Advanced Device Technology, University of Science & Technology, Daejeon 34113, Republic of Korea

Abstract

It is generally believed that in first-order phase transitions in materials with imperfections, the formation of phase domains must be affected to some extent by stochastic (probabilistic) processes. The stochasticity would lead to unreliable performance in nanoscale devices that have the potential to exploit the transformation of physical properties in a phase transition. Here we show that stochasticity at nanometer length scales is completely suppressed in the thermally driven metal-insulator transition (MIT) in sputtered vanadium dioxide (VO_2) films. The nucleation and growth of domain patterns of metallic and insulating phases occur in a strikingly reproducible way. The *completely deterministic* nature of domain formation and growth in films with imperfections is a fundamental and unexpected finding about the kinetics of this material. Moreover, it opens the door for realizing reliable nanoscale devices based on the MIT in VO_2 and similar phase change materials.

The metal-insulator transition (MIT) in vanadium dioxide (VO_2) [1–3] has the potential to lead to a number of disruptive technologies, including ultra-fast data storage, optical switches, resistive random access memory (RRAM) and transistors which move beyond the limitations of silicon [4–6]. For

applications, VO_2 films are deposited on crystalline substrates to prevent cracks observed in bulk VO_2 crystals across the thermally driven MIT. Near the MIT, VO_2 films exhibit coexistence between metallic and insulating phases at nanometer length scales [7–9], which opens up further potential applications such as memristors, tunable capacitors, [10–13] and optically engineered devices such as perfect absorbers [14].

The phenomenon of phase coexistence is quite broadly observed across strongly correlated condensed matter systems, occurring for example, in the high-T_c superconducting cuprates [15,16], the colossal magnetoresistive manganites [17–19], as well as the oxides of vanadium [7,9,20–22]. Highly ordered patterns [9,15,16,19,22] result in response to long range interactions. Generally speaking, the spatial periodicity of these patterns ranges from very small (nanometers or less) [15,16] for strong interactions, such as Coulomb interaction between domains, to hundreds of nanometers or more for somewhat weaker interactions [9,19,21,22] such as long-range elastic mismatch with a substrate. The increasing periodicity as the interaction strength decreases is attributed to the free energy cost of forming the boundary between domains. In this regime, stochastic processes such as fluctuations between phases [23] or irreproducibility in the domain pattern upon thermal cycling [21] have been observed. In contrast, amorphous patterns emerge when imperfections disrupt the long range interaction [7,18]. Generally speaking, there is sparse experimental data on the nanoscale spatial reproducibility of these patterns near phase transitions in solids with imperfections.

Due to the stochastic nature of nucleation of a new phase during a first order phase transition [24–26], it was expected that stochasticity constituted an inherent challenge to creating reproducible phase transition based devices on the scale of the domain size. Until now, the expectation for these systems was that although regions may preferentially transition due to inhomogeneity and defects, some degree of irreproducibility was unavoidable [18,21,27]. The primary result of this work is the discovery of completely reproducible patterns of metallic and insulating phase domains in a VO_2 film. Remarkably,

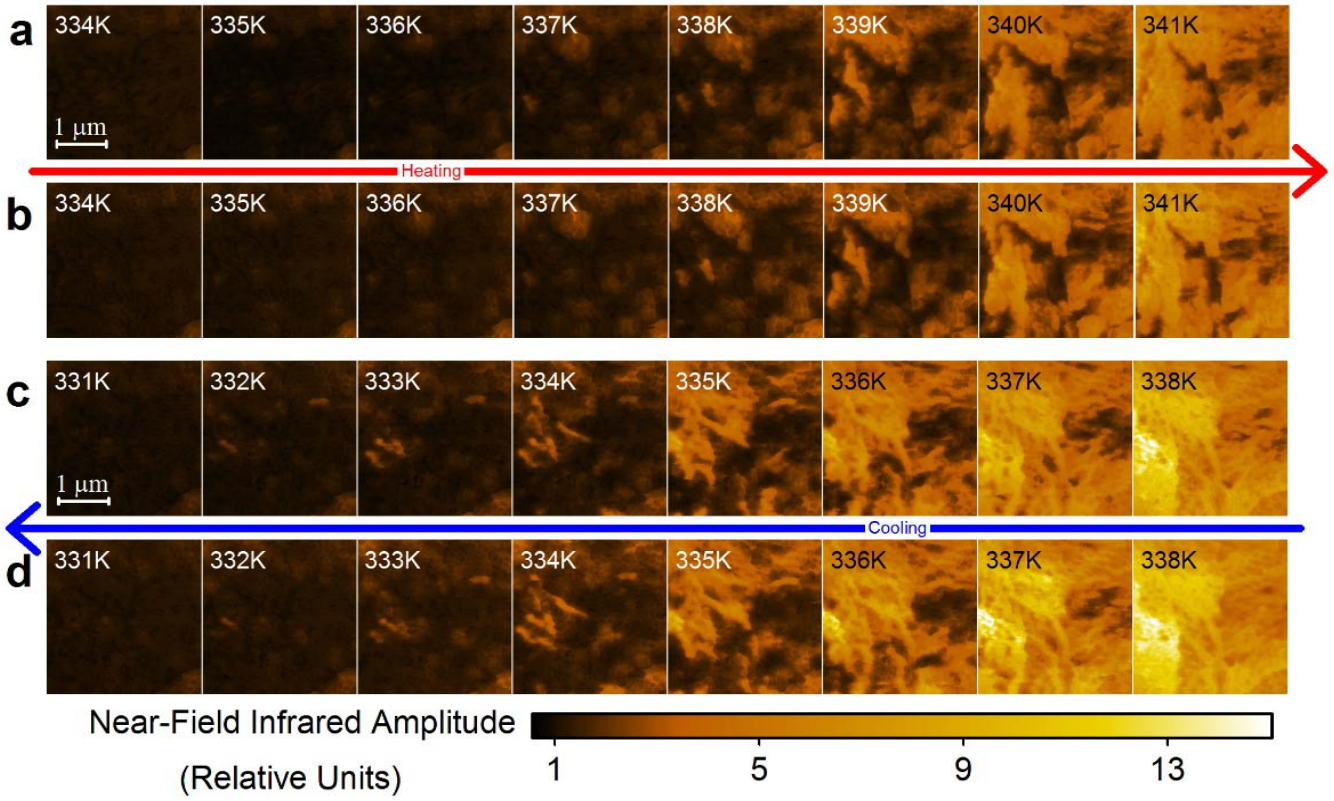

Figure 1. Near-field infrared amplitude images of the same region at different temperatures are displayed. Higher infrared amplitude corresponds to metallic regions, while lower signals correspond to insulating regions. The signals are normalized to the average signal of the completely insulating 329 K image (not shown). Rows a and b show separate heating runs. Rows c and d show separate cooling runs.

nucleation of phase domains as well as their propagation is found to be highly repeatable. Insight gained through our work could be applied to VO_2 and across the entire range of similar correlated materials, whose novel phase transitions have tremendous potential for technological impact [28]. The primary finding in this Letter is obtained with the technique of scattering-type scanning near-field infrared microscopy (S-SNIM). This technique was utilized to image the patterns formed by coexisting metallic and insulating domains in the thermally driven MIT in a sputtered VO_2 film. We achieved unprecedented spatial stability over a broad temperature range which allowed us to obtain S-SNIM images in the same area of the film for repeated heating and cooling runs.

In this work, we study a 45 nm thick VO_2 film grown by radio frequency (RF) sputtering on (0001) sapphire. Growth conditions and characterization of films similar to the one studied in this work are reported in Ref. [29]. At room temperature, the VO_2 film is in the M_1 phase with (010) orientation as

seen in X-ray diffraction data included in supplemental material [30]. A scanning electron microscopy (SEM) image of the film shows grains with non-trivial shapes [30]. Such films have distinct topographic features, in the form of "valleys" or "crevices" between grains as measured by atomic force microscopy [30]. The "valleys" are reasonably interpreted as grain boundaries. These films are ideal for our purpose because topographic features can be used to ensure that the infrared images are consistently taken in the same microscopic area.

The S-SNIM data presented in this work was obtained on a neaSNOM microscope from Neaspec GmbH. In S-SNIM, infrared light is scattered from a metal coated tip of a tapping mode atomic force microscope (AFM) [31]. The scattered light contains information about the optical near-field interaction between the tip and the region of the sample immediately below the tip. The AFM-based technique allows for the simultaneous collection of topographic and optical images of a given region of the film, with spatial resolution on the order of the AFM tip radius, approximately 15 to 20 nm. The pseudo-heterodyne detection scheme and demodulation of the optical signals at higher harmonics of the tip oscillation frequency are used to reduce various background contributions [31,32]. The near-field infrared amplitude data presented in this work was obtained from the third harmonic demodulation of the infrared signal. The S-SNIM technique is primarily sensitive to the local dielectric function at the incident infrared wavelength. However, the local topography can influence the signal, i.e. the signal is generally higher in a valley than on a topographic peak. This surface roughness (~ 3 nm RMS) induced S-SNIM contrast can be seen in the low temperature (purely insulating) images, and causes a variation of about 10%. The laser wavelength of 10.6 μm used in this work is within the band gap of insulating VO_2, and above the infrared-active phonon region. The large change in optical constants across the MIT at this wavelength results in significant infrared contrast between metallic regions (high infrared signal) and insulating regions (low infrared signal), much greater than that caused by the topography [7,8,20].

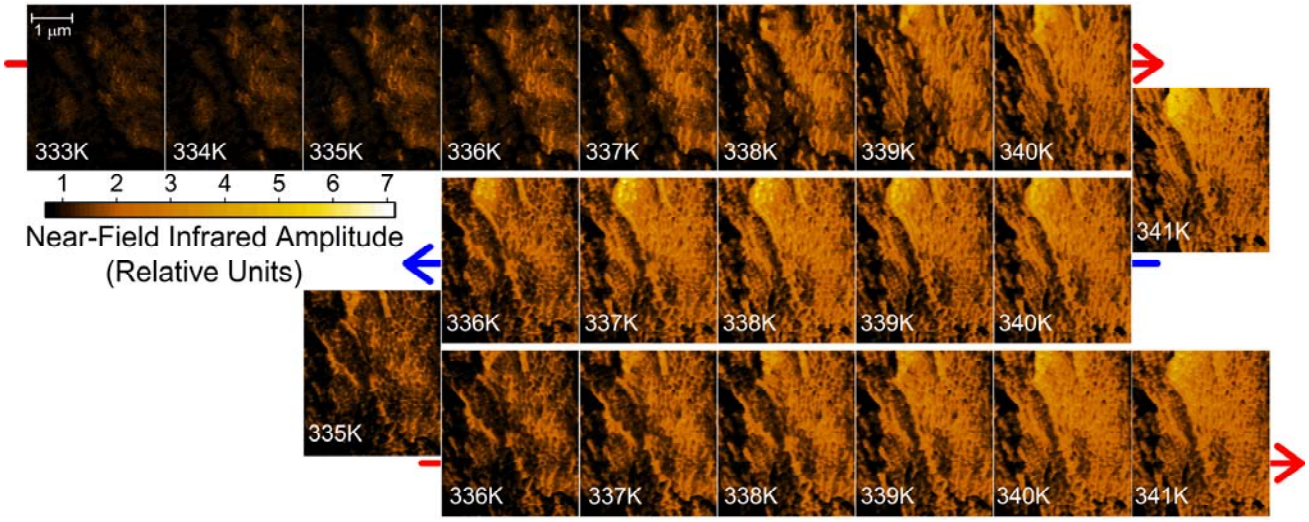

Figure 2. Near-field infrared amplitude images are obtained during a non-monotonic temperature cycle through the phase coexistence regime. Arrows denote either heating (red) or cooling (blue). The near-field infrared amplitude is normalized to that of the insulating phase in each image. The area scanned here is different from the one shown in Figure 1.

It is clear that the S-SNIM images presented here are due to the MIT because they are temperature dependent while the topography is temperature independent.

For S-SNIM measurements at elevated temperatures, spatial drift of the scan area upon changing temperature was minimized [30] by placing the sample at the center of a circular heating stage which was designed in-house. A silicon diode thermometer and a resistive heating element were mounted on the stage and these components along with a Lakeshore model 335 temperature controller were employed for thermal management. A slow temperature ramp rate ~ 0.2 K/minute was used to minimize overshoot (< 0.1 K) from the set-point temperature. Minute differences in this overshoot can result in an image that appears somewhat more progressed in one run as opposed to another. Once the set point temperature is obtained, it is held stable within 0.1 K for the full duration of the S-SNIM scan.

Representative S-SNIM images obtained in the same spatial region are presented in Fig. 1. Each row represents a separate heating or cooling run through the phase coexistence regime. The nucleation and growth of phase domain patterns are reproducible for the heating runs and the cooling runs respectively. Note that somewhat different patterns are observed in the heating runs compared to the

97 cooling runs. As seen previously in polycrystalline VO_2 films, the MIT is percolation-type in which phase
98 domains first nucleate and then grow in amorphous, fractal-like patterns [7,8,20]. The patterns are
99 static and stable in time, provided the temperature is held constant. The significant advance over
100 previous works is our finding that phase domains nucleate and grow reproducibly in separate thermal
101 runs through the MIT. Deterministic factors that are "quenched", or frozen into the film at the time of
102 growth, alone dictate nucleation and domain patterns. While the variance introduced by this "quenched
103 disorder" can be treated as random in theoretical models [33], this does not in any way imply that phase
104 domain formation is necessarily a stochastic physical process.

105 The S-SNIM images were taken over a number of runs through the metal-insulator transition. To
106 investigate the reproducibility of the phase domain patterns, raster scans were taken in the same area
107 of the film in repeated thermal runs. We performed two heating runs in three different regions of the
108 film for a total of six heating runs. In none of the regions was any evidence of irreproducibility observed.
109 Three cooling runs were performed at the location shown in Fig. 1 to compare the patterns to the
110 heating runs in the same location and to verify the repeatability for cooling. The three cooling runs
111 showed reproducible patterns of coexisting phases (two of the three cooling runs are shown in Fig. 1). In
112 all of the above runs, the sample was first brought to a temperature completely outside of the phase
113 coexistence regime where it was fully metallic (for cooling) or fully insulating (for heating).

114 To obtain further insight into the domain pattern formation, we report a non-monotonic
115 temperature cycle through the phase coexistence regime in a common area of the film in Fig. 2.
116 Interestingly, although the same pattern reemerges at 341 K, the phase domain patterns on the two
117 heating portions of the cycle are quite different. Hence, it is not necessary to exit the coexistence regime
118 to reset the memory of the system.

We emphasize that nucleation occurs at precisely the same location in each uni-directional, monotonic temperature excursion across the MIT (See Fig. 3 b,c,d, and e). As the sample temperature crosses the equilibrium temperature, where the free energies of both phases are equal, it is thermodynamically preferred to form a domain ($\Delta G_{Domain}<0$). Kinetically, however, the always positive

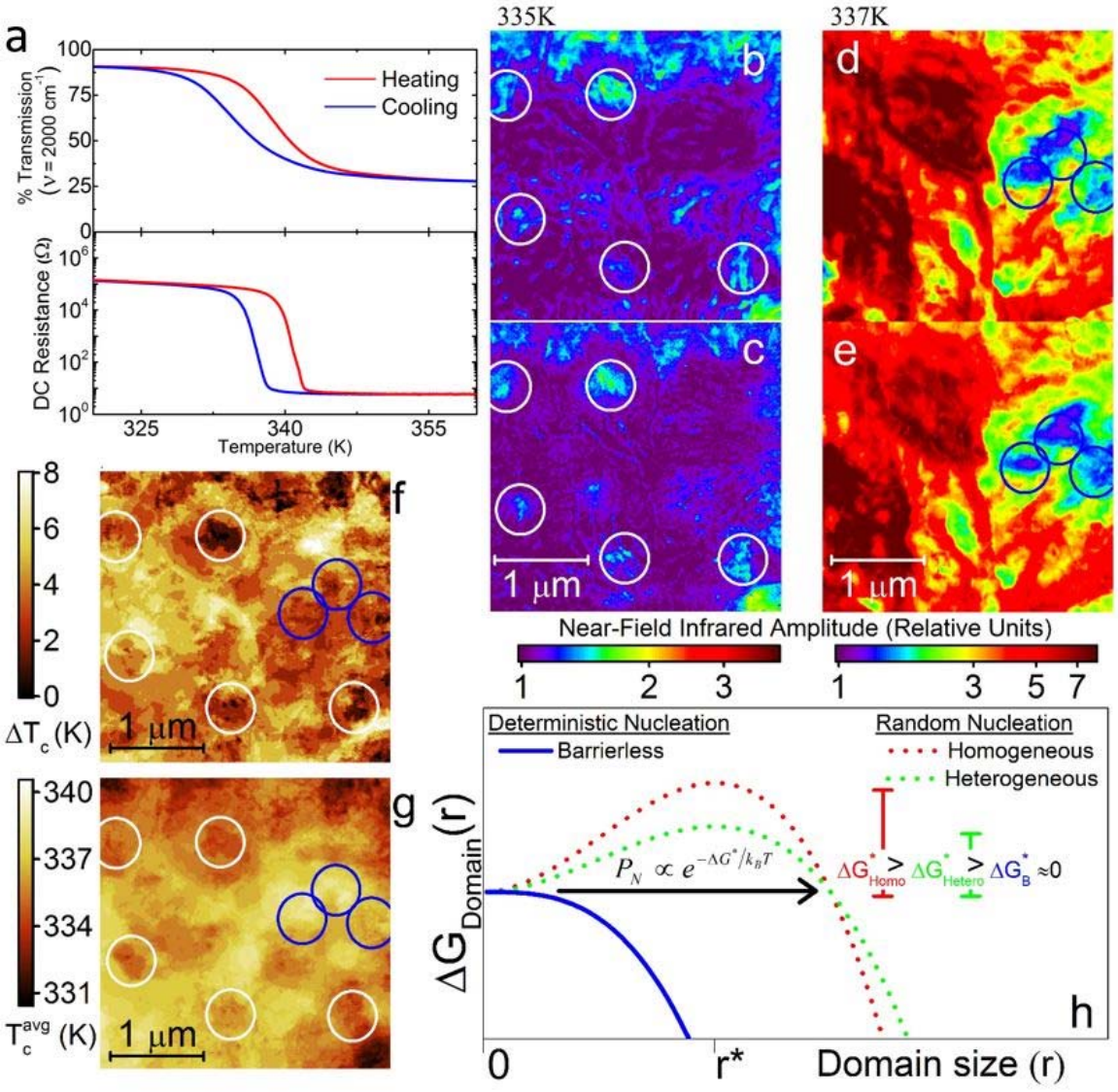

Figure 3 a**:** Macroscopic thermal hysteresis loop measured via infrared transmission through the film-substrate system (upper panel) and dc resistance of the film (lower panel). Panels b,c,d,e: S-SNIM images demonstrating the nucleation sites on heating (b and c**),** and cooling (d and e) of the same area as shown in Fig. 1. Panels f and g**:** Local hysteresis width (ΔT_c) and local phase equilibrium temperature (T_c^{avg}) respectively for the area shown in b,c,d,e. White (blue) circles in b,c,d,e,f,g serve to guide the eye to some of the nucleation sites which occur on heating (cooling). Panel **h:** Schematic of the free energy landscape for a domain of characteristic linear dimension *r* for different types of nucleation sites. Here we make the distinction between heterogeneous nucleation and "barrierless nucleation". Barrierless nucleation is a special case of heterogeneous nucleation where, unlike the more general case, the nucleation barrier is completely removed, and nucleation occurs deterministically.

strain and interfacial free energy terms oppose the formation of domains below a critical size (r*). Thus, any new domain must pass (tunnel) through the nucleation barrier (ΔG*). This tunneling is an inherently stochastic process. Nucleation occurs at each site in a given time interval with a probability (P_N) proportional to $e^{-\Delta G^*_{local}/k_B T}$ (See Fig 3h) [24]. This pertains to homogeneous nucleation, which occurs in the homogeneous bulk, as well as heterogeneous nucleation which occurs at an imperfection such as an atomic defect or a grain boundary. In heterogeneous nucleation, the free energy of forming the critical nucleus can be altered significantly thereby reducing the barrier to nucleation. Nevertheless, as long as a barrier to nucleation exists, the process is expected to be inherently stochastic. Thus, it is quite surprising that stochastic nucleation is not observed in our experiments. In the analysis and discussion that follows, we deduce and explain qualitative features of the phase transition kinetics implied by our observations.

Quenched disorder locally alters the free energy balance between the phases [34]. As a result, the *local* temperature where the free energy of both phases is equal $\left(T_{eq}^{local}\right)$ is shifted from the bulk value. As neither phase is thermodynamically preferred at this temperature, some degree of superheating or undercooling is in general necessary to overcome the nucleation barrier. It is natural to consider an elementary (local) hysteresis loop, where each pixel in the S-SNIM images of the scanned area has both a heating and cooling transition temperature. Equivalently, each pixel is characterized by a hysteresis width (ΔT_c) – the difference between the heating and cooling transition temperatures - and an average of the transition temperatures (T_c^{avg}). The hysteresis width ΔT_c is related the local degree of undercooling and overheating required to drive the transition, and is thus characteristic of the local nucleation barrier. The average transition temperature (T_c^{avg}) is a measure of T_{eq}^{local}, if one assumes that the local degree of undercooling and overheating is the same ($\frac{1}{2}\Delta T_c$). While one could consider a more complicated model, which includes interactions such as strain between domains [35], the re-

emergence of the same 341 K pattern from different histories (Fig. 2) indicates that this simple model is sufficient. We note that nucleation occurs at sites where the local ΔT_c is suppressed (See Fig 3f), which confirms that the nucleation barrier is greatly reduced, if not completely removed, at these sites. At these "optimal" nucleation sites, the MIT can proceed along a barrierless (or nearly barrierless) path, and hence occurs reliably (see Fig. 3h). That no stochastic domain formation is observed is strong evidence that the nucleation barrier (ΔG_{local}) away from the optimal sites is significantly higher. We observe that, on heating, nucleation occurs at optimal sites where the local equilibrium temperature (T_c^{avg}) is relatively low. Conversely, on cooling, nucleation occurs at optimal sites where T_c^{avg} is relatively high (See Fig. 3 b,c,d,e,f and g). The optimal sites for nucleation on heating are different from the ones on cooling, and this explains the differences in phase domain patterns upon heating and cooling (see Fig. 1). Note that to determine the local transition temperatures in Fig. 3, we employ a threshold of 1.45 for the normalized infrared amplitude, above which the pixel is considered to be metallic. We define the local transition temperature as the temperature where the signal first crosses the threshold for both the heating and cooling directions. The observed local characteristics (See Fig. 3 f and g) – and thus our conclusions – do not change appreciably for a broad range of reasonable thresholds. Appropriate thresholds are those that exceed the slight topography-induced optical contrast, but are still low enough to capture the noticeable optical contrast due to nucleation. Both ΔT_c and T_c^{avg} contribute to the shape of the thermal hysteresis loop observed in macroscopic measurements of the MIT. Factors such as the strain cost associated with larger domains, the presence of grain boundaries, and inhomogeneity in T_c^{avg} isolate phase domains and limit their growth. The delayed propagation of the new phase results in a broad transition width and hysteresis width as seen in the infrared transmission measurement and the dc resistance data (Fig. 3a). These factors are less pronounced in single crystals. Therefore, VO_2 single crystals have very sharp transitions and don't exhibit

phase coexistence unless subject to external strain [36–39]. In such crystals, the finite hysteresis width (not to be confused with the transition width) is set by the smallest local ΔT_c.

Interestingly, reports in the literature suggest that there is a correlation between the size of VO_2 single crystals and the width of the hysteresis. It is found that the width of the hysteresis of the MIT can be increased greatly, to as much as 35 K for single domain VO_2 nano-particles [40,41]. The hysteresis width is systematically lessened in nano-particles with increasing size and number of grain boundaries [41]. This trend holds for free-standing VO_2 crystallites, from the somewhat larger VO_2 "nanorods" [42] - which have a hysteresis width of approximately 5-10 K - to millimeter scale free-standing VO_2 crystals which have hysteresis widths of approximately 2 K [43]. A small single domain VO_2 nanoparticle is unlikely to contain an optimal nucleation site. The huge hysteresis widths observed in these crystallites are a clear indication that the nucleation barrier at nearly all sites is so large that stochastic nucleation processes occur rarely, if at all. In sputtered VO_2 films, the dramatic separation between the nucleation barrier at the optimal sites and at all other sites ultimately leads to nucleation that is *functionally deterministi*c: nucleation occurs reliably - only at the optimal sites - each time the temperature crosses T_{eq}^{local}.

There is clear evidence in our work [30] and in the literature [20,41,44] that grain boundaries play a role in the formation of optimal sites. VO_2 films with nanoscale grains have almost negligible macroscopic hysteresis widths, which is indicative of abundant nucleation sites [44]. It has been suggested previously via DFT+U calculations that oxygen vacancies at grain boundaries serve to catalyze the MIT [41]. Moreover, there is experimental evidence that oxygen vacancies lead to reduced T_c [45,46]. The accumulating evidence clearly indicates that clusters of oxygen vacancies at grain boundaries serve as optimal nucleation sites.

To conclude, we have shown that phase domain nucleation and propagation are completely deterministic processes in the thermally driven MIT in a sputtered VO_2 film. In such films, quenched disorder can be used to reliably control the spatial distribution and propagation of phase domains. Interestingly, nanoscale spatial inhomogeneity in the ultra-fast optically driven MIT [27,47] suggests that our conclusion can be generalized to the MIT driven by optical pulses. Our work provides a platform for further meaningful exploration into reliable nanoscale VO_2 electronic and photonic devices.

Acknowledgments

MMQ acknowledges support from NSF (grant # DMR-1255156). TJH, DJL, and MMQ are grateful to Tobias Gokus of Neaspec GmbH for technical support for the neaSNOM instrument and the infrared nano-imaging setup.

References

* Corresponding author: mumtaz@wm.edu

[1] M. Imada, A. Fujimori, and Y. Tokura, Rev. Mod. Phys. **70**, 1039 (1998).

[2] A. Perucchi, L. Baldassarre, P. Postorino, and S. Lupi, J. Physics-Condensed Matter **21**, 323202 (2009).

[3] D. N. Basov, R. D. Averitt, D. van der Marel, M. Dressel, and K. Haule, Rev. Mod. Phys. **83**, 471 (2011).

[4] S. Hormoz and S. Ramanathan, Solid. State. Electron. **54**, 654 (2010).

[5] H. Zhou, J. Li, Y. Xin, G. Sun, S. Bao, and P. Jin, Ceram. Int. **42**, 7655 (2016).

[6] T. Slusar, J. C. Cho, B. J. Kim, S. J. Yun, and H. T. Kim, APL Mater. **4**, 26101 (2016).

[7] M. M. Qazilbash, M. Brehm, B.-G. Chae, P.-C. Ho, G. O. Andreev, B.-J. Kim, S. J. Yun, A. V Balatsky, M. B. Maple, F. Keilmann, H.-T. Kim, and D. N. Basov, Science **318**, 1750 (2007).

[8] M. M. Qazilbash, M. Brehm, G. O. Andreev, A. Frenzel, P.-C. Ho, B.-G. Chae, B.-J. Kim, S. J. Yun, H.-T. Kim, A. V Balatsky, O. G. Shpyrko, M. B. Maple, F. Keilmann, and D. N. Basov, Phys. Rev. B **79**, 75107 (2009).

[9] M. K. Liu, M. Wagner, E. Abreu, S. Kittiwatanakul, a. McLeod, Z. Fei, M. Goldflam, S. Dai, M. M. Fogler, J. Lu, S. A. Wolf, R. D. Averitt, and D. N. Basov, Phys. Rev. Lett. **111**, 96602 (2013).

[10] T. Driscoll, H.-T. Kim, B.-G. Chae, M. Di Ventra, and D. N. Basov, Appl. Phys. Lett. **95**, 43503 (2009).

[11] L. Pellegrino, N. Manca, T. Kanki, H. Tanaka, M. Biasotti, E. Bellingeri, A. S. Siri, and D. Marre, Adv. Mater. **24**, 2929 (2012).

[12] Z. Yang, C. Ko, V. Balakrishnan, G. Gopalakrishnan, and S. Ramanathan, Phys. Rev. B **82**, 205101 (2010).

[13] W. A. Vitale, L. Petit, C. F. Moldovan, M. Fernandez-Bolanos, A. Paone, A. Schuler, and A. M. Ionescu, Sens. Actuat A-Phys **241**, 245 (2016).

[14] M. A. Kats, D. Sharma, J. Lin, P. Genevet, R. Blanchard, Z. Yang, M. M. Qazilbash, D. N. Basov, S. Ramanathan, and F. Capasso, Appl. Phys. Lett. **101**, (2012).

[15] T. Hanaguri, C. Lupien, Y. Kohsaka, D. H. Lee, M. Azuma, M. Takano, H. Takagi, and J. C. Davis, Nature **430**, 1001 (2004).

[16] M. Vershinin, S. Misra, S. Ono, Y. Abe, Y. Ando, and A. Yazdani, Science **303**, 1995 (2004).

[17] L. W. Zhang, C. Israel, A. Biswas, R. L. Greene, and A. de Lozanne, Science **298**, 805 (2002).

[18] K. Lai, M. Nakamura, W. Kundhikanjana, M. Kawasaki, Y. Tokura, M. A. Kelly, Z.-X. Shen, P. G. Radaelli, R. M. Ibberson, D. N. Argyriou, H. Casalta, K. H. Andersen, S.-W. Cheong, J. F. Mitchell, K. Lai, M. Nakamura, W. Kundhikanjana, M. Kawasaki, Y. Tokura, M. A. Kelly, and Z.-X. Shen, Science **329**, 190 (2010).

[19] J. Dho, Y. N. Kim, Y. S. Hwang, J. C. Kim, and N. H. Hur, Appl. Phys. Lett. **82**, 1434 (2003).

[20] A. Frenzel, M. M. Qazilbash, M. Brehm, B.-G. Chae, B.-J. Kim, H.-T. Kim, A. V Balatsky, F. Keilmann, and D. N. Basov, Phys. Rev. B **80**, 115115 (2009).

[21] M. Liu, M. Wagner, J. Zhang, A. McLeod, S. Kittiwatanakul, Z. Fei, E. Abreu, M. Goldflam, A. J. Sternbach, S. Dai, K. G. West, J. Lu, S. A. Wolf, R. D. Averitt, and D. N. Basov, Appl. Phys. Lett. **104**, 121905 (2014).

[22] A. S. McLeod, E. van Heumen, J. G. Ramirez, S. Wang, T. Saerbeck, S. Guenon, M. Goldflam, L. Anderegg, P. Kelly, A. Mueller, M. K. Liu, I. K. Schuller, and D. N. Basov, Nat. Phys. **13**, 80 (2017).

[23] V. Podzorov, C. H. Chen, M. E. Gershenson, and S.-W. Cheong, Europhys. Lett. **55**, 411 (2001).

[24] R. W. Balluffi, S. Allen, and W. C. Carter, *Kinetics of Materials* (Wiley, 2005).

[25] I. Ford and V. Kalikmanov, *Nucleation Theory* (Cambridge University Press, 2004).

[26] S. Karthika, T. K. Radhakrishnan, and P. Kalaichelvi, Cryst. Growth Des. **16**, 6663 (2016).

[27] B. T. O'Callahan, A. C. Jones, J. Hyung Park, D. H. Cobden, J. M. Atkin, and M. B. Raschke, Nat. Commun. **6**, 6849 (2015).

[28] J. Rensberg, S. Zhang, Y. Zhou, A. S. McLeod, C. Schwarz, M. Goldflam, M. Liu, J. Kerbusch, R. Nawrodt, S. Ramanathan, D. N. Basov, F. Capasso, C. Ronning, and M. A. Kats, Nano Lett. **16**, 1050 (2016).

[29] S. J. Yun, J. W. Lim, J.-S. S. Noh, B.-J. J. Kim, and H.-T. T. Kim, Jpn. J. Appl. Phys. **48**, 04C139 (2009).

[30] *See Supplemental Material at* (n.d.).

[31] F. Keilmann and R. Hillenbrand, Philos. Trans. A. Math. Phys. Eng. Sci. **362**, 787 (2004).

[32] N. Ocelic, A. Huber, and R. Hillenbrand, Appl. Phys. Lett. **89**, 101124 (2006).

[33] S. Liu, B. Phillabaum, E. W. Carlson, K. A. Dahmen, N. S. Vidhyadhiraja, M. M. Qazilbash, and D. N. Basov, Phys. Rev. Lett. **116**, 36401 (2016).

[34] Y. Imry and M. Wortis, Phys. Rev. B **19**, 3580 (1979).

[35] J. G. Ramírez, A. Sharoni, Y. Dubi, M. E. Gómez, and I. K. Schuller, Phys. Rev. B - Condens. Matter Mater. Phys. **79**, 1 (2009).

[36] J. H. Park, J. M. Coy, T. S. Kasirga, C. Huang, Z. Fei, S. Hunter, and D. H. Cobden, Nature **500**, 431 (2013).

[37] J. Wei, Z. Wang, W. Chen, and D. H. Cobden, Nat. Nanotechnol. **4**, 420 (2009).

[38] B. S. Mun, K. Chen, Y. Leem, C. Dejoie, N. Tamura, M. Kunz, Z. Liu, M. E. Grass, C. Park, J. Yoon, Y. Y. Lee, and H. Ju, Phys. Status Solidi - Rapid Res. Lett. **5**, 107 (2011).

[39] B. S. Mun, K. Chen, Y. Leem, C. Dejoie, N. Tamura, M. Kunz, Z. Liu, M. E. Grass, C. Park, J. Yoon, Y. Y. Lee, and H. Ju, Phys. Status Solidi - Rapid Res. Lett. **9**, 206 (2015).

[40] R. Lopez, L. A. Boatner, T. E. Haynes, R. F. Haglund, and L. C. Feldman, Appl. Phys. Lett. **79**, 3161 (2001).

[41] K. Appavoo, D. Y. Lei, Y. Sonnefraud, B. Wang, S. T. Pantelides, S. a Maier, and R. F. Haglund, Nano Lett. **12**, 780 (2012).

[42] J. Cao, E. Ertekin, V. Srinivasan, W. Fan, S. Huang, H. Zheng, J. W. L. Yim, D. R. Khanal, D. F. Ogletree, J. C. Grossman, and J. Wu, Nat. Nanotechnol. **4**, 732 (2009).

[43] T. Kong, M. W. Masters, S. L. Bud'ko, and P. C. Canfield, APL Mater. **3**, 41502 (2015).

[44] J. Y. Suh, R. Lopez, L. C. Feldman, and R. F. Haglund, J. Appl. Phys. **96**, 1209 (2004).

[45] S. Fan, L. Fan, Q. Li, J. Liu, and B. Ye, Appl. Surf. Sci. **321**, 464 (2014).

[46] H. Y. Xu, Y. H. Huang, S. Liu, K. W. Xu, F. Ma, and P. K. Chu, RSC Adv. **6**, 79383 (2016).

[47] S. A. Donges, O. Khatib, B. T. O'Callahan, J. M. Atkin, J. H. Park, D. Cobden, M. B. Raschke, S. A. Donges, O. Khatib, B. T. O'Callahan, J. M. Atkin, J. H. Park, D. Cobden, and M. B. Raschke, Nano Lett. **16**, 3029 (2016).